PCCP

Thickness dependent homogeneous crystallization of ultrathin amorphous solid water films

Journal:	*Physical Chemistry Chemical Physics*
Manuscript ID	CP-ART-11-2019-005981.R1
Article Type:	Paper
Date Submitted by the Author:	31-Dec-2019

Complete List of Authors:	Harada, Kuniaki; Kyoto University 杉本, 敏樹; Institute for Molecular Science, ; JST, Kato, Fumiaki; Kyoto University; Institute for Molecular Science Watanabe, Kazuya; Kyoto University, Chemistry Matsumoto, Yoshiyasu; TPCRI

Thickness dependent homogeneous crystallization of ultrathin amorphous solid water films

Author names

*Kuniaki Harada,[a] Toshiki Sugimoto,[*bc] Fumiaki Kato,[ab] Kazuya Watanabe,[a] and Yoshiyasu Matsumot[d]*

Author address

[a] Department of Chemistry, Graduate School of Science, Kyoto University, Kyoto 606-8502, Japan.

[b] Institute for Molecular Science, Okazaki, Aichi 444-8585, Japan.

[c] Precursory Research for Embryonic Science and Technology (PRESTO), Japan Science and Technology Agency (JST), Saitama 332-0012, Japan.

[d] Toyota Physical and Chemical Research Institute, Nagakute, Aichi 480-1192, Japan.

Abstract

The crystallization mechanism and kinetics of amorphous materials are of paramount importance not only in basic science but also in the application field because it is closely related to their thermal stability. In the case of amorphous nanomaterials, thermal stability distinctively different from that of bulk materials often emerges. Despite intensive studies in the past, a thorough understanding of the stability at the molecular level has not been reached particularly on how crystallization processes depend on size and are influenced by their surface and interface. In this article, we report the film-size-dependent crystallization of thermally relaxed nonporous ASW ultrathin films on a Pt(111) surface as a benchmark system of amorphous molecular films. The crystallization processes at the surface and interior of the ASW ultrathin films are monitored simultaneously with thermal desorption and infrared reflection absorption, respectively, as a function of the film thickness. Here, we demonstrate that the crystallization is initiated solely by "homogeneous nucleation" irrespective of the film thickness while the crystallization rate remarkably depends on the thickness; the rate of 5-layer (~1.5 nm) ASW films is one order of magnitude higher than that of 20-layer (~6 nm) films. Moreover, we found a clear correlation between the film-thickness-dependent crystallization kinetics and microscopic structural disorder associated with the broad distribution of hydrogen-bond length between water molecules.

1. Introduction

The crystallization of amorphous materials is generally triggered by spontaneous creation of crystalline nuclei. Two processes are distinguishable in terms of the place where crystallized nuclei are formed: *heterogeneous nucleation* at the surface of material or the interface with the other material, and *homogeneous nucleation* in the bulk. Moreover, the crystallization processes depend on the system size. In particular, amorphous nanofilms,[1-16] nanoparticles,[17,18] and nanowires[19-21] often show thermal stability distinctively different from thick films and bulk solids. Despite the intensive studies in the past, it has been poorly understood at the molecular level how the crystallization mechanism and the kinetics of amorphous nanomaterials depend on the size and are affected by the presence of surface and interface. This stems from the inherent difficulty in investigating the microscopic structure of interfacial amorphous nanomaterials with conventional experimental techniques such as x-ray and neutron diffraction. Therefore, it is highly challenging to obtain detailed molecular-level insights into the crystallization processes of nanoscopic amorphous solids.

In the case of water ice, the amorphous nanofilms are typically prepared by vapor deposition on cooled substrate below 110 K. Such a metastable form of ice is commonly referred to as amorphous solid water (ASW).[22-25] For over a quarter century, ASW film has been the subject of intense studies for unveiling anomalous physical and thermodynamic properties of liquid water[26-35] as well as for exploring crystallization processes of interfacial water.[1-6,36-44] ASW film is also known as a dominant solid substance covering dust particles in interstellar space,[45,46] where the ASW mantle with a typical thickness of 5 nm coexists with a partially crystallized form of ice.[47,48] Surfaces of the ultrathin ASW and crystalline ice (CI) mantles play crucial roles in stimulating molecular evolution and spin-isomer conversion[49-51] which are

particularly important in astrochemical and astrophysical environments. Because the interaction of molecules with ice significantly depends on the surface local structure, it is of crucial importance whether the surface of nanoscopic ice film is amorphous or crystallized.

In a vast body of mechanistic studies, atomically flat substrates have been typically used as a model support for ASW films.[1-7,26,27,36-40,42,43,49,52-65] In particular, the most stable face of platinum, Pt(111), on which ASW film is grown smoothly in the layer-by-layer mannar,[7,57-59] has provided a key platform for investigating the unique physicochemical properties of ASW films.[1-4,7,26,37,52,55-62] In the case of ASW films thicker than ~50 monolayer (ML), it has been typically reported that the crystallization proceeds via homogeneous nucleation followed by three-dimensional growth of the generated nuclei.[2,5,26,36,61,66] In contrast, the crystallization kinetics and the mechanism of ASW ultrathin films (< ~50 ML) have been poorly understood at the molecular level. In particular, it remains ambiguous how the finite film size affects the crystallization kinetics,[6,7] and the crystallization mechanisms proposed so far are contradictory to each other.[1-5,44,67] Namely, heterointerface-induced nucleation was proposed on the basis of thickness-dependent behavior of the isothermal desorption (ITD) rate of ASW ultrathin films,[1-4] while surface-induced nucleation was proposed on the basis of the temperature-programmed desorption (TPD) rate of $CHCl_3$ from ASW films with 45 ML thickness.[44] In contrast, a molecular-dynamics simulation predicted homogeneous nucleation on flat substrates such as Pt(111) that strongly interacts with water molecules.[67] Therefore, further experimental studies are required for a comprehensive understanding of the crystallization mechanism of ASW ultrathin films.

In this paper, we report a firm mechanism of crystallization for the ASW ultrathin films on the benchmark model Pt(111) substrate on the basis of systematic observation of the

crystallization kinetics of the ASW films as a function of film thicknesses from 5 to 50 ML using in-situ infrared reflection absorption spectroscopy (IRAS) and thermal desorption measurements (TPD and ITD) simultaneously. IRAS has great advantages over conventional diffraction techniques in sensitivity and non-invasive characterization of the amorphous and crystalline structure of ultrathin ice films.[6,26,27,36,38,42,44,52,53,56,63,64,66,68-85] The simultaneous measurements of IRAS and thermal desorption enable us to investigate the crystallization kinetics of the entire ASW film and of its surface. With this approach, we succeeded in elucidating the crystallization mechanism of the ASW nanofilms definitely: the crystallization proceeds via *homogeneous nucleation* irrespective of the film thickness while the crystallization rate depends on film thickness remarkably. Moreover, we demonstrate that the observed film-thickness-dependent kinetics is well correlated with microscopic structural disorder associated with the broad distribution of hydrogen-bond length between water molecules.

2. Experimental

The experiments were performed in an ultrahigh vacuum (UHV) chamber pumped down to a base pressure of $< 5 \times 10^{-8}$ Pa. A Pt(111) disc with 10 mm in diameter and 1 mm thickness was spot-welded to two Ta wire leads attached on a liquid nitrogen cooled sample holder. The sample can be heated to 1200 K by resistive heating and cooled to 105 K. The temperature was monitored within an experimental error less than ±1 K by a calibrated type-K thermocouple spot-welded to the back of the sample disc. The Pt(111) surface was cleaned by cycles of Ar^+ ion sputtering with 0.5 keV followed by annealing to 1000 K for 10 minutes, annealing at 750 K in 2×10^{-5} Pa of O_2 for 30-60 minutes, and flash annealing to 1030 K. The surface cleanliness and structure of the substrate were checked by using X-ray photoelectron spectroscopy (XPS), low-

energy electron diffraction (LEED), respectively. XPS spectra revealed that the substrate was chemically clean without any trace of oxygen and carbon contaminants; LEED revealed a clear 1×1 pattern with the three-fold symmetry characteristic of a (111) surface of face-centered cubic metal.

As water gas sources, we used pure H_2O (milli-Q) and isotopically diluted HDO water. D_2O water with an isotopic purity of 99.96 atom % D purchased from ISOTEC and H_2O were mixed to obtain H diluted HDO water. HDO concentration in the D_2O rich water vapor was estimated to be ~10 mol% ([OH]/[OD] ratio ~0.05) with a quadrupole mass spectrometer (QMS: Balzers/Pfeiffer Vacuum QME-200 Prisma). These water samples were carefully pre-degassed in a UHV gas line by repeating freeze-pump-thaw cycles. Thermally relaxed nonporous ASW and CI films were grown on Pt(111) by backfilling water-vapor deposition at the substrate temperatures of 110 and 135 K, respectively, with a deposition rate of ~0.02 ML/s. In this article, the adsorbed amount of water molecules is expressed in the monolayer (ML) unit in which 1 ML corresponds to the amount of water adsorbed in the saturated first layer with the $(\sqrt{39}\times\sqrt{39})R16.1^{\circ}$ superstructure on Pt(111);[57,86,87] this is nearly equivalent to the amount of water molecules in a layer of the ASW film with a thickness of ~0.3 nm[58] and a density of ~1×10^{15} molecules/cm^2.[59]

The amount of water molecules adsorbed on Pt(111) was carefully determined by the TPD technique.[68,88] TPD measurements were conducted using a QMS with a home-built small cup extended from QMS at ~3 mm in front of the sample surface. Water adsorbates at a saturation coverage of the first layer showed a quasi-zero order desorption peak at ~162 K for H_2O under a heating rate of 0.1 K/s; this result is consistent with previous studies.[57,68,86-89] Desorption of water at around 200 K that is derived from the dissociated water molecules on

Pt(111)[60,90] has never been observed. Because the area of a desorption peak is proportional to the amount of adsorbed water molecules, the adsorbed amount of a multilayer ASW and CI film was derived by comparing the peak area of the TPD curve for the saturated first layer. The uncertainty in film thickness with this method was evaluated to be less than 10 %.[88]

IRAS was conducted with a Fourier transform infrared spectrometer (Brucker IFS 66v/S).[88] The non-polarized IR light was focused on the sample surface by a concave mirror through a BaF_2 view port at an incident angle of 84°. The reflected light from the sample was detected with a mercury cadmium telluride detector (Teledyne Judson Technologies). The light path outside the UHV chamber was evacuated below 1 Pa to avoid unfavourable IR absorption by H_2O and CO_2 gas in air. IRAS spectra $1 - R(\omega)/R_0(\omega)$ were measured with a resolution of 4 cm^{-1}, where $R(\omega)$ and $R_0(\omega)$ are the reflected signals from the surface with and without adsorbed water, respectively. Any appreciable IRAS spectra derived from contaminants have never been observed during the ice-film deposition and crystallization experiments.

3. Results and discussion

3.1. Crystallization mechanism

Figure 1a shows the TPD traces of 18 ML ASW and 20 ML CI films at a heating rate of 0.1 K/s. The desorption rate of the ASW film suddenly decreases at ~150 K, and the TPD trace follows that of the CI film above 154 K. Because the activation energy for desorption E_{des} of ASW films is lower than that of CI films by ~1.4 kJ/mol,[26,52,55,91] the desorption rate declines when the surface is crystallized. The significant drop so called "bump" in the TPD trace has thus been considered as a signature of crystallization at the surface of ASW films.[6,26,37-41,52,55,56,63,91-93] Although the crystallization of ASW films was accompanied with dewetting,[94,95] it was reported

that the contribution of dewetting to the observed sudden drops of the desorption rate is much smaller than that of crystallization.[36,57] Thus, Figure 1a indicates that water molecules desorb from amorphous surface below 150 K while they desorb from crystalline surface above 154 K; the surface crystallization of the ASW film with 18 ML initial thickness starts at ~150 K and completed at ~154 K. This crystallization process also manifests itself in spectral changes in IRAS. Figure 1b shows the peak normalized IRAS spectra of the OH-stretching band measured for the ASW sample with initial thickness of 18 ML in the temperature range from 110 to 158 K. The spectral shape of the ASW film starts to change at ~150 K and converges toward that of CI films above ~154 K. Note that the crystallized ice show the same IRAS spectrum as the crystalline ice film with the same thickness grown on 135 K; this is because ASW films crystallize to form the same microscopic structure and morphology with the as-grown crystalline ice film.[1] Therefore, our results clearly indicate that crystallization occurs at surface and inside of the 18 ML ASW film almost simultaneously in the experimental time scale of 40 s during the heating from 150 to 154 K at 0.1 K/s.

To quantitatively compare the temperature dependence of crystallinity at surface with that in bulk, we evaluated a fraction crystallized at surface, $x_{surf}(T)$, from TPD traces and that in bulk, $x_{bulk}(T)$, from IRAS spectra as follows.[26,36,42,44,53,66,69] The temperature dependence of the desorption rate, $R(T)$, is expressed with a linear combination of the two desorption rates of water from ASW surface $R_{ASW}(T)$ and from CI surface $R_{CI}(T)$ obtained independently,[26,53]

$$R(T) = x_{surf}(T) \cdot R_{CI}(T) + \{1 - x_{surf}(T)\} \cdot R_{ASW}(T). \quad (1)$$

From eq 1, $x_{surf}(T)$ is derived as, $x_{surf}(T) = (R_{ASW}(T) - R(T))/(R_{ASW}(T) - R_{CI}(T))$. Similarly IRAS spectra, $S(\omega, T)$, is expressed with a linear combination of ASW and CI components as

$$S(\omega, T) = x_{bulk}(T) \cdot S_{CI}(\omega) + \{1 - x_{bulk}(T)\} \cdot S_{ASW}(\omega), \quad (2)$$

where $S_{CI}(\omega)$ and $S_{ASW}(\omega)$ are IRAS spectra of CI and ASW films, respectively. $x_{bulk}(T)$ is derived from the curve fitting (Figure S1), in which the thickness dependence of the spectral shape of each component (Figure S2) is taken into account (see Supplementary information Sec. 1 for details). The IRAS spectra measured during the crystallization process were well reproduced by a sum of the contributions from ASW and CI domains (Figure S1).

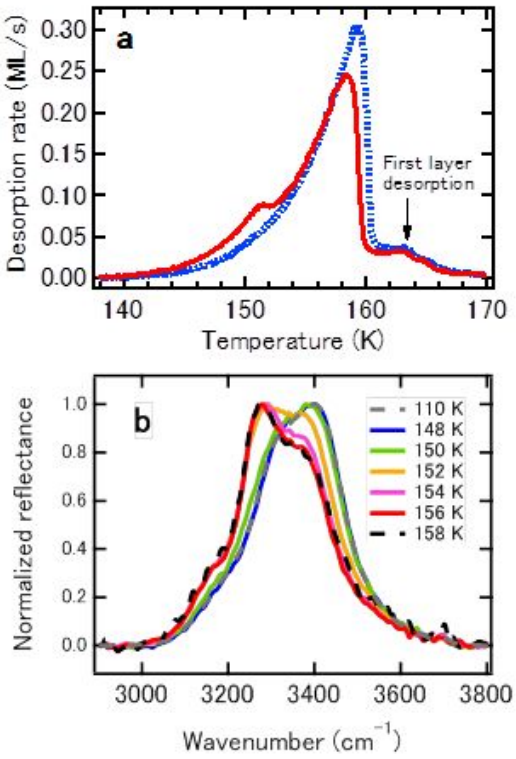

Figure 1. Simultaneous monitoring of surface and bulk crystallization processes. (a) TPD traces of 18 ML H_2O ASW film grown at 110 K (solid line) and 20 ML H_2O CI film grown at 135 K (dotted line) on Pt(111). The heating rate is 0.1 K/s. (b) Peak normalized IRAS spectra for the 18 ML ASW film simultaneously measured during the TPD process. Accuracy of the temperature is within 1 K.

Figure 2 shows how x_{surf} and x_{bulk} change with temperature for 9, 18, 27, and 45 ML ASW films; x_{surf} and x_{bulk} varied with temperature very similarly in all the films investigated. For these thin films, no temperature gradient is expected across the sample under the heating

condition (0.1 K/s) and on the experimental time scale.[96,97] If the crystallization rate were dominated by heterogeneous nucleation at the vacuum/ASW interface (ASW surface) or at the ASW/Pt(111) interface, the temperature dependence of x_{surf} should be different from that of x_{bulk}. On the contrary, the temperature dependence of x_{surf} derived from TPD rates is similar to x_{bulk} derived from the IRAS spectra. Moreover, similar time evolutions of x_{surf} and x_{bulk} were observed in the isothermal crystallization process (Figure S3b). These results firmly indicate that the ASW ultrathin films crystallize via homogeneous nucleation.

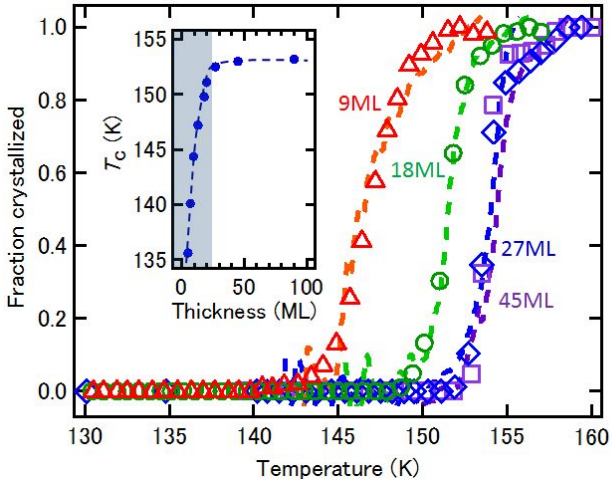

Figure 2. Temperature dependence of the fraction crystallized at the surface x_{surf} obtained by TPD (dashed lines) and that in the entire film x_{bulk} obtained by IRAS (symbols) for 9 ML (red triangle), 18 ML (green circle), 27 ML (blue diamond) and 45 ML (purple square). (inset) Thickness dependence of crystallization temperature T_c defined as a temperature at $x_{bulk} = x_{surf} = 0.1$.

Note that the microscopic structure including porosity does not affects crystallization kinetics and mechanism; Kay *et al*. have demonstrated that the porous and non-porous ASW films (100 ML) deposited on Pt(111) at 20 K and 80 K, respectively, show almost the same crystallization kinetics as the thermally relaxed non-porous ASW film (100 ML) deposited on

Pt(111) at 110 K.[52] In addition, we confirmed that the deposition rate does not affect the crystallization kinetics and mechanism of ASW ultrathin films; the ASW ultrathin film deposited with a rate of 0.3 ML/s show almost the same homogeneous nucleation and crystallization process as those deposited with a rate of 0.02 ML/s (Figure S4).

The heterogeneous nucleation mechanism initiated at the ASW/Pt(111) interface was proposed only on the basis of the ITD measurements,[1-4,41] in which the completing time of surface crystallization τ_c was substantially extended as the thickness of ASW films increases from ~5 to ~50 ML. In fact, the isothermal measurements of the current study well reproduced their results as shown in Figure S5a. However, we emphasize here that these results do not contradict the *homogeneous nucleation* mechanism; it is not possible to determine the nucleation mechanism only by the thermal desorption measurements because they provide the information of crystallization only at the *surface* of ASW films. Note that the current study probed crystallization not only at the surface by thermal desorption (ITD and TPD) but also that of the entire film by IRAS. Therefore, the simultaneous changes in x_{surf} and x_{bulk} are firm evidence to conclude that the crystallization of ultrathin ASW films on Pt(111) is initiated simultaneously in the film and at the surface via *homogeneous* nucleation rather than via heterogeneous nucleation. The crystallization mechanisms of ASW ultrathin films grown on Au(111) and Ru(0001)[5] were assumed to be in line with our homogeneous-nucleation mechanism although simultaneous monitoring of x_{surf} and x_{bulk} was not conducted for these ASW films.

Theoretical studies of ice nucleation at interface with metal[67,98,99] have reported that heterogeneous nucleation is significantly affected by the structure of interfacial water; if water molecules near the interface form a hexagonal hydrogen-bond network (6-membered rings) similar to the crystalline phase, the interfacial nucleation can be substantially promoted at the

interface.[67,98,99] However, this is not the case for the ASW films on Pt(111). It has been demonstrated that the interfacial water molecules, i.e. first-layer water interacting directly with Pt(111), form a topologically highly deformed superstructure with 5- and 7-membered rings as well as 6-membered rings.[1,100-103] The vibrational signature derived from the strong hydrogen bonds of the superstructure was observed at ~1965 cm^{-1} in the water monolayer grown at 110 K (Figure S7).[100,101,104] Thus, the strong hydrogen bonds with topologically deformed network of first-layer water on Pt(111) would suppress the preferential nucleation at the ASW/Pt(111) interface as theoretically predicted.[67] The preferential nucleation at the vacuum/ASW interface (surface) can also be inhibited due to the significant deviation from the hexagonal structure, i.e. most of water molecules at the surface of the ASW form 4- and 5-membered rings.[70] Moreover, we have recently demonstrated that the *topmost surface layer of CI* forms disordered amorphous-like hydrogen-bond network between 120 and 200 K.[105] Therefore, heterogeneous nucleation is not the right crystallization mechanism for the ASW ultrathin films below 50 ML on Pt(111).

A couple of studies have proposed the surface-induced (heterogeneous) nucleation mechanism for ASW films. First, Backus et al. claimed that this mechanism is operative for the ASW nanofilms (45 ML) grown on a slanted platinum substrate with wide terraces of (111) face[44] on the basis of the TPD of $CHCl_3$ molecules adsorbed on the ASW surfaces. It should be emphasized that the desorption temperature of $CHCl_3$ (130-145 K) is much higher than those of N_2 (T_d: 25-45 K)[61] and CHF_2Cl (T_d: 85-105 K)[54,65] typically used for probing x_{surf}. The relatively strong interaction of $CHCl_3$ with the ASW surface stimulates nucleation at the ASW film surface[62] as HCl molecule does;[56] thus, TPD of $CHCl_3$ is not suitable for the probe of the crystallinity at ice surfaces.[62] Second, surface-initiated *heterogeneous nucleation* was recently proposed for thick ASW films (100-1000 ML) grown on a 50-ML thick substrate of decane

molecules on Pt(111),[53,64] in contrast to the previous reports suggesting that thick ASW films (~100 ML) grown directly on metal substrates, including Pt(111) substrate, typically crystallize via *homogeneous nucleation*.[2,5,26,36,52,61,66] Although the heterogeneous nucleation has been discussed to be an inherent nucleation mechanism of thick ASW films in ref. 53 and 64, such a thick decane substrate may have significant impact on heat accumulation and crystallization kinetics in the upper ASW films.[78,106] Much lower thermal conductivity of thick decane substrate than metal substrates may cause less efficient dissipation of heat of adsorption of water molecules during water-vapor deposition, resulting in local heating and some thermal annealing around the growing surface of the thick ASW films.[106] Thus, the upper side of the thick ASW films on the decane substrate would accelerate crystallization preferentially around the film surface, resulting in "top-down" crystallization.[53,64] In the case of ASW films directly grown on metal substrates, this heat accumulation would be significantly suppressed. Therefore, the *homogeneous nucleation* is the most plausible mechanism for the crystallization of the thin ASW films on Pt(111).

3.2. Thickness dependent homogeneous crystallization

The other notable feature is that the onset temperature of crystallization markedly depends on film thickness below ~20 ML (Figure 2) although nucleation itself proceeds *homogeneously* in all the films investigated; the crystallization temperature T_c defined as a temperature at $x_{bulk} = x_{surf} = 0.1$ markedly increases with film thickness and levels off at around ~20 ML (inset of Figure 2). Almost the same thickness dependence of the crystallization temperature was observed for D_2O ASW films below ~20 ML (Figure S6), indicating that nuclear quantum effects is not relevant to the overall thickness dependent profiles of the crystallization kinetics.

To gain deeper insights into this size effect on the crystallization kinetics, we analyzed the kinetics of isothermal crystallization of ASW films with the Avrami equation[107-109] given by

$$x(t) = 1 - \exp[-(kt)^n], \quad (3)$$

where x, t, and k represent the fraction crystallized, the elapsed time, and the crystallization rate constant, respectively. The Avrami index n is a parameter related to the crystallization mechanism. The Avrami theory describes isothermal homogeneous crystallization with two growth rates: J, the formation rate of crystalline nuclei and G, the volume growth rate of crystalline nuclei, i.e. $x(t) = 1 - \exp[-\alpha(Jt) \times (Gt)^m]$, where m and α represent the dimensionality of crystalline domain growth and the geometrical factor of crystalline nuclei, respectively. Thus, k^n is proportional to JG^m and $n = m + 1$.

Figure 3a displays the thickness dependence of x_{bulk} at 145 K as a function of elapsed time, indicating that the crystallization process markedly depends on film thickness; the time required for completing crystallization, τ_c, increases with film thickness (Figure S5). All the crystallization curves were well fitted by the Avrami equation. Figure 3b shows the thickness dependence of n. For the ASW films thicker than ~20 ML, n is about 4; the crystallization proceeds via homogeneous nucleation followed by the three-dimensional growth of the generated nuclei, which is in good agreement with the results reported in previous works for ASW films thicker than ~50 ML,[2,5,26,36,52,61,66] including 100- and 150-ML thick ASW films on Pt(111).[26,52,61]

In contrast, n decreases monotonically from 4 to 1 below ~20 ML. This decrease in n is reasonable because crystalline domains in the ultrathin films grow and reach soon the surface and/or the interface of the films and the three-dimensional growth would be inhibited.[110-113] In particular, n becomes 1 as the thickness is 5 ML, indicating 0 dimensional growth in which

overall crystallization is completed only at the stage of generating crystalline nuclei. From this result, the critical size (diameter) of crystalline nuclei is estimated to be about 5 molecules (~1.5 nm). Our estimation is in good agreement with the prediction of classical nucleation theory and molecular dynamics simulations of amorphous ice and liquid water,[2,98,114-117] indicating that the crystalline nuclei is formed by cooperative rearrangement of sizeable ensembles of the order of ~5^3 molecules.[114,118]

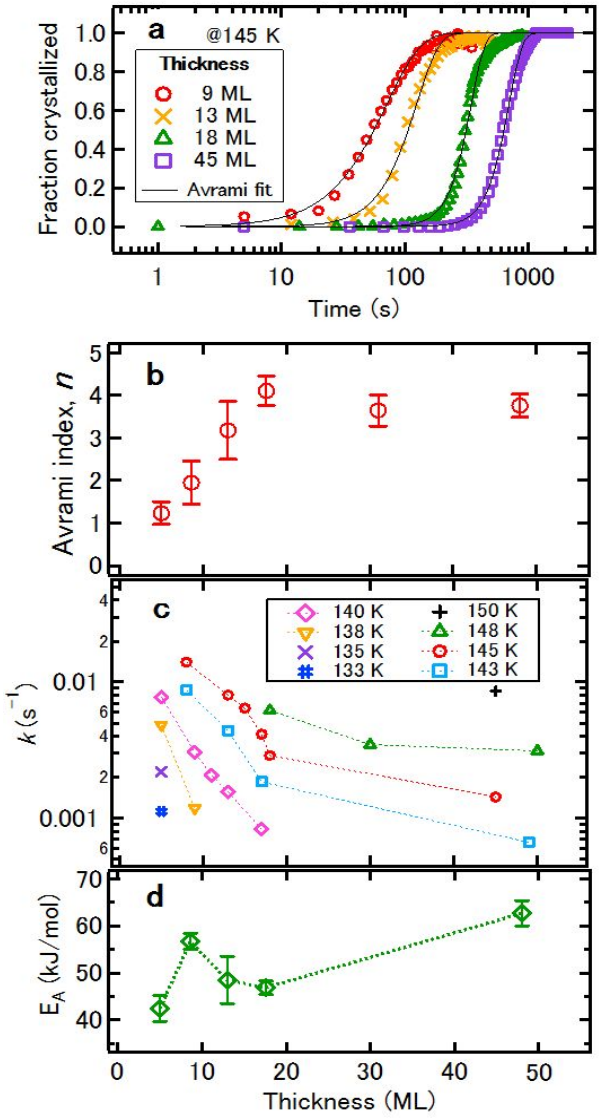

Figure 3. Isothermal crystallization of ASW ultrathin films on Pt(111). (a) Time evolution of the fraction crystallized at 145 K obtained by IRAS for various thicknesses. Results of curve fitting with Avrami equation is shown by black lines. Thickness dependence of (b) Avrami index n, (c) crystallization rate constant k, and (d) apparent activation energy E_A obtained by the Arrhenius plot of k shown in Figure S8a.

In addition to n, k also depends on film thickness as shown in Figure 3c. While n increases monotonically from 1 to 4 with increasing film thickness, k decreases dramatically. The substantial increases in T_c (inset of Figure 2) and τ_c (Figure S5) with film thickness correspond to the dramatic decrease in k (Figure 3c). Thickness dependence of the apparent activation energy E_A (Figure 3d) was derived from the Arrhenius plots of k (Figure S8a). Because k^n is proportional to JG^m, E_A is given by the sum of the activation energy for nucleation E_N and crystalline growth E_G as

$$E_A = \frac{E_N + mE_G}{n} = \frac{E_N + (n-1)E_G}{n}. \quad (4)$$

Although the present experiments do not allow us to determine E_N and E_G independently, E_N = 43 $\pm$ 3 kJ/mol is derived from E_A at the 5 ML ASW film (n =1) because the relation $E_N = E_A$ is satisfied for n =1. This value is by a factor of ~ 4 smaller than E_N = 155±15 kJ/mol reported previously for thick ASW films,[36,61,65] suggesting that E_N and possibly E_G for the *thermally relaxed ASW ultrathin films* are not constant and dependent on the film thickness (see also Supplementary Information Sec. 5).

3.3. Correlation between microscopic structure and crystallization rate

On the basis of our experimental results, a fundamental question arises: why does the rate of homogeneous-nucleation induced crystallization markedly depend on the ASW film thickness? Because thermodynamics and kinetics of nucleation are influenced sensitively by local hydrogen-bond environments, this question is pertinent to the hydrogen-bond network in the ultrathin ASW films. To shed light on the microscopic hydrogen-bond structure, we conducted IRAS measurements of isotope diluted HDO ASW ultrathin films with various thicknesses. In contrast to neat H_2O ice, intramolecular vibrational coupling in HDO and

intermolecular coupling among OH moieties are negligibly small in the isotope diluted HDO ice; thus, this makes the hydrogen-bonded OH-stretch bands of ice very simple,[68,71-73] and the wavenumber of a localized OH oscillator of isotope diluted ice has been well correlated to the intermolecular distance of O-H···O hydrogen-bond ($R_{O\text{-}O}$).[74-76]

Figure 4a shows the peak normalized IRAS spectra of the hydrogen-bonded OH-stretching band of the thermally relaxed HDO ASW films grown on Pt(111) at 110 K. The peak position is almost independent of the film thickness while the band becomes broader as the film is thinner. The spectral deformation due to the optical interference is not responsible for the ultrathin films below 50 ML.[71,88] In general, as a O-H ··· O hydrogen-bond connecting a neighboring molecule becomes stronger, the stretching frequency of the OH bond involved in the hydrogen bond decreases.[68,71,76,119] Using the relation between the stretching frequency and $R_{O\text{-}O}$ (Figure 4b), the distributions of spectral intensity is converted to those of $R_{O\text{-}O}$ as shown in Figure 4c, in which the oscillator strength of OH stretch of HDO molecule is assumed to be independent of the local hydrogen-bond structure in the films.[73] This thickness dependent distribution of $R_{O\text{-}O}$ (Fig. 4d) indicates that the thinner films contain a larger fraction of water molecules whose $R_{O\text{-}O}$ is shorter or longer than the average hydrogen-bond distance, $\langle R_{O-O} \rangle$ ~ 2.78 Å, than the thicker films. Therefore, the hydrogen-bond networks are more disordered and fluctuated[35,118] in the thinner films; the hydrogen-bond structure in the entire films changes flexibly and cooperatively with their film thickness below ~20 ML as was typically reported in small metal clusters.[120] These pronounced features can be responsible for the high values of k and the resultant small T_c and τ_c for the thinner ASW films.

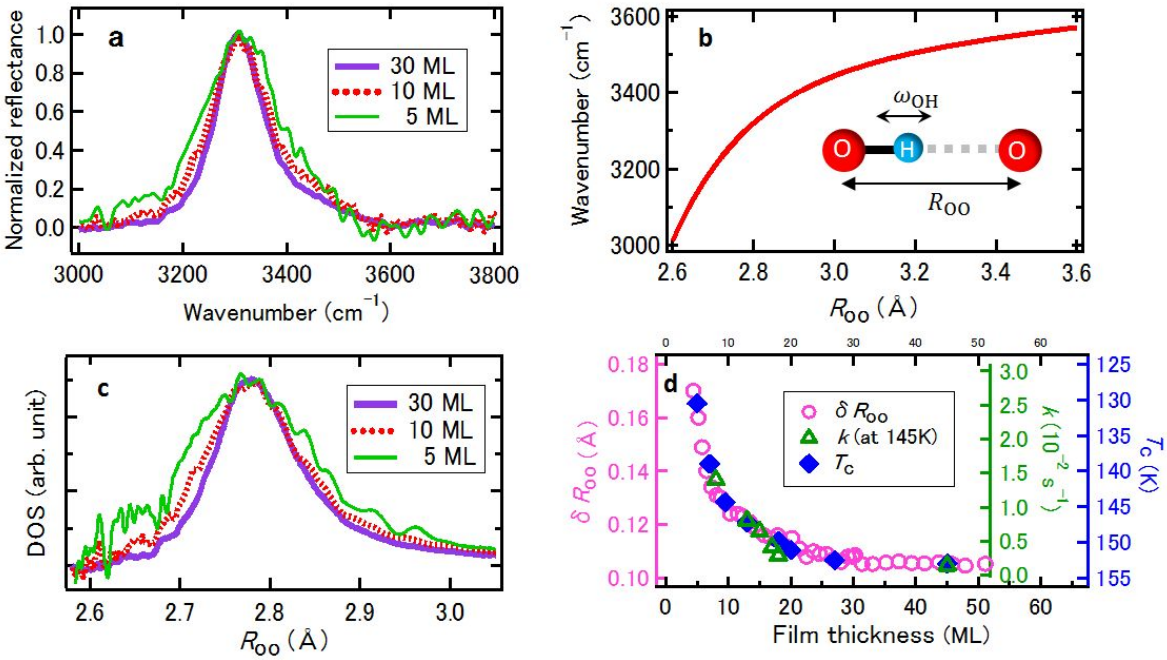

Figure 4. (a) Peak normalized IRAS spectra of isotope diluted HDO ASW ultrathin films on Pt(111) grown and measured at 110 K. (b) Relation between frequency of the hydrogen-bonded OH stretching mode of isotope diluted HDO molecule and the intermolecular hydrogen-bond distance.[74-76] (c) Peak normalized distribution of $R_{O\text{-}O}$ for 5 ML (thick solid line), 10 ML (dotted line) and 30 ML (thin solid line). (d) Correlation between thickness dependent crystallization temperature T_c (diamond), crystallization rate constant k at 145 K (triangle), and dispersion of hydrogen-bond distance δR_{oo} (circle) derived from the full width of half maximum of IRAS spectra.

4. Conclusions

In summary, some important outcomes have emerged from the simultaneous measurements of thermal desorption (TPD and ITD) and IRAS regarding the crystallization of ultrathin ASW films grown on a model Pt(111) substrate at 110 K. First, the crystallization of these ultrathin films proceeds via homogeneous nucleation with a critical diameter of the nuclei of about five molecules (~1.5 nm); these findings unambiguously resolve the conflict on the

nucleation mechanism in the benchmark ASW ultrathin films on Pt(111). Second, the rate of crystallization initiated by the homogeneous nucleation markedly increases with decreasing the film thickness below ~20 ML, accompanying significant decrease in crystallization temperature T_c and the completing time of surface crystallization τ_c. Third, the thickness dependences of T_c, τ_c and the crystallization rate constant k are well correlated with that of the band width of the isotope diluted OH stretching band, i.e., the distribution of intermolecular distance R_{oo}. This implies that the thermally relaxed hydrogen-bond structures of ASW ultrathin films are more disordered and fluctuated as the film is thinner. The pronounced structural disorder and fluctuation in the ultrathin hydrogen-bond network facilitates homogeneous nucleation and destabilizes the ASW films thermally. Our results provide a new insight into the film-size-dependent crystallization of ASW thin films.

Conflicts of interest

There are no conflicts to declare.

Abbreviations

ASW, amorphous solid water; CI, crystalline ice; ITD, isothermal desorption; TPD, temperature-programmed desorption; IRAS, infrared reflection absorption spectroscopy

Author information

*Correspondence should be addressed to T.S. E-mail: toshiki-sugimoto@ims.ac.jp.

Acknowledgment

We are grateful to Nao Okumura, Norihiro Aiga, Yuji Otsuki and Tetsuya Hama for fruitful discussions. This work was supported by JSPS KAKENHI Grant-in-Aid for Scientific Research (A), No. 19H00865 and 16H02249; Grant-in-Aid for Specially Promoted Research, No. 17H06087; Grant-in-Aid for JSPS Research Fellow, No. 17J08362; JST, PRESTO Grant Number JPMJPR16S7, Japan.

Notes and references

1 Zimbitas, G.; Haq, S.; Hodgson, A. The Structure and Crystallization of Thin Water Films on Pt(111). *J. Chem. Phys.* 2005, **123**, 174701.

2 Ahlström, P.; Löfgren, P.; Lausma, J.; Kasemo, B.; Chakarov, D. Crystallization Kinetics of Thin Amorphous Water Films on Surfaces: Theory and Computer Modeling. *Phys. Chem. Chem. Phys.* 2004, **6**, 1890-1898.

3 Löfgren, P.; Ahlström, P.; Lausma, J.; Kasemo, B.; Chakarov, D. Crystallization Kinetics of Thin Amorphous Water Films on Surfaces. *Langmuir* 2003, **19**, 265-274.

4 Löfgren, P.; Ahlström, P.; Chakarov, D. V.; Lausmaa, J.; Kasemo, B. Substrate Dependent Sublimation Kinetics of Mesoscopic Ice Films. *Surf. Sci.* 1996, **367**, L19-L25.

5 Smith, R. S.; Huang, C.; Wong, E. K. L.; Kay, B. D. Desorption and Crystallization Kinetics in Nanoscale Thin Films of Amorphous Water Ice. *Surf. Sci.* 1996, **367**, L13-L18.

6 May, R. A.; Smith, R. S.; Kay, B. D. Probing the Interaction of Amorphous Solid Water on a Hydrophobic Surface: Dewetting and Crystallization Kinetics of ASW on Carbon Tetrachloride. *Phys. Chem. Chem. Phys.* 2011, **13**, 19848-19855.

7 Kimmel, G. A.; Petrik, N. G.; Dohnálek, Z.; Kay, B. D. Crystalline Ice Growth on Pt(111) and Pd(111): Nonwetting Growth on a Hydrophobic Water Monolayer. *J. Chem. Phys.* 2007, **126**, 114702.

8 Zacharias, M.; Streitenberger, P. Crystallization of Amorphous Superlattices in the Limit of Ultrathin Films with Oxide Interfaces. *Phys. Rev. B* 2000, **62**, 8391-8396.

9 Bloch, L.; Kauffmann, Y.; Pokroy, B. Size Effect on the Short Range Order and the Crystallization of Nanosized Amorphous Alumina. *Cryst. Growth Des.* 2014, **14**, 3983-3989.

10 Kužel, R.; Nichtová, L.; Matéj, Z.; Musil, J. In-situ X-ray Diffraction Studies of Time and Thickness Dependence of Crystallization of Amorphous TiO_2 Thin Films and Stress Evolution. *Thin Solid Films* 2010, **519**, 1649-1654.

11 Wang, X.; Rein, M.; Vlassak, J. J. Crystallization Kinetics of Amorphous Equiatomic NiTi Thin Films: Effect of Film Thickness. *J. Appl. Phys.* 2008, 103, 023501.

12 Raoux, S.; Jordan-Sweet, J. L.; Kellock, A. J. Crystallization Properties of Ultrathin Phase Change Films. *J. Appl. Phys.* 2008, **103**, 114310.

13 Li, L.; Song, S.; Zhang, Z.; Zhu, Y.; Song, Z.; Cheng, Y.; Lv, S.; Liu, B.; Chen, L. Thickness Dependent Nano-Crystallization in $Ti_{0.43}Sb_2Te_3$ Films and Its Effect on Devices. *Thin Solid Films* 2015, **590**, 13-16.

14 Pellegren, J. P.; Sokalski, V. M. Thickness and Interface-Dependent Crystallization of CoFeB Alloy Thin Films. *IEEE Trans. Magn.* 2015, **51**, 3400903.

15 Martínez-Tong, D. E.; Vanroy, B.; Wübbenhorst, M.; Nogales, A.; Napolitano, S. Crystallization of Poly($_L$-lactide) Confined in Ultrathin Films: Competition between Finite Size Effects and Irreversible Chain Adsorption. *Macromolecules* 2014, **47**, 2354-2360.

16 Vanroy, B.; Wübbenhorst, M.; Napolitano, S. Crystallization of Thin Polymer Layers Confined between Two Adsorbing Walls. *Macro Lett.* 2013, **2**, 168-172.

17 Caldwell, M. A.; Raoux, S.; Wang, R. Y.; Wong, H. S. P.; Milliron, D. J. Synthesis and Size-Dependent Crystallization of Colloidal Germanium Telluride Nanoparticles. *J. Mater. Chem.* 2010, **20**, 1285-1291.

18 Hirasawa, M.; Orii, T.; Seto, T. Size-Dependent Crystallization of Si Nanoparticles. *Appl. Phys. Lett.* 2006, **88**, 093119.

19 Lee, S. H.; Jung, Y.; Agarwal, R. Highly Scalable Non-Volatile and Ultra-Low-Power Phase-Change Nanowire Memory. *Nat. Nanotechnol.* 2007, **2**, 626-630.

20 Lee, S. H.; Jung, Y.; Agarwal, R. Size-Dependent Surface-induced Heterogeneous Nucleation Driven Phase-Change in $Ge_2Sb_2Te_5$ Nanowires. *Nano. Lett.* 2008, **8**, 3303-3309.

21 Lee, S. H.; Ko, D. K.; Jung, Y.; Agarwal, R. Size-Dependent Phase Transition Memory Switching Behavior and Low Writing Currents in GeTe Nanowires. *Appl. Phys. Lett.* 2006, **89**, 223116.

22 Burton, E. F.; Oliver, W. F. The Crystal Structure of Ice at Low Temperatures. *Proc, Roy. Sci. Ser. A* 1935, **153**, 166-172.

23 Dowell, L. G.; Rinfret, A. P. Low-Temperature Forms of Ice as Studied by X-Ray Diffraction. *Nature* 1960, **188,** 1144-1148.

24 Olander, D. S.; Rice, S. A. Preparation of Amorphous Solid Water. *Proc. Natl. Acad. Sci. USA* 1972, **69**, 98-100.

25 Hallbrucker, A.; Mayer, E.; Johari, G. P. Glass-Liquid Transition and the Enthalpy of Devitrification of Annealed Vapor-Deposited Amorphous Solid Water: A Comparison with Hyperquenched Glassy Water. *J. Phys. Chem.* 1989, **93**, 4986-4990.

26 Smith, R. S.; Matthiesen, J.; Knox, J.; Kay, B. D. Crystallization Kinetics and Excess Free Energy of H_2O and D_2O Nanoscale Films of Amorphous Solid Water. *J. Phys. Chem. A* 2011, **115**, 5908-5917.

27 Xu, Y.; Petrik, N. G.; Smith, R. S.; Kay, B. D.; Kimmel, G. A. Growth Rate of Crystalline Ice and the Diffusivity of Supercooled Water from 126 K to 262 K. *Proc. Natl. Acad. Soc. USA* 2016, **113**, 14921-14925.

28 Johari, G. P.; Fleissner, G.; Hallbrucker, A.; Mayer, E. Thermodynamic Continuity between Glassy and Normal Water. *J. Phys. Chem.* 1994, **98**, 4719-4725.

29 Mishima, O.; Stanley, H. E. The Relationship between Liquid, Supercooled and Glassy Water. *Nature* 1998, **396**, 329-335.

30 Ito, K.; Moynihan, C. T.; Angell, C. A. Thermodynamic Determination of Fragility in Liquids and a Fragile-to-Strong Liquid Transition in Water. *Nature* 1999, **398**, 492-495.

31 Angell, C. A. Insights into Phases of Liquid Water from Study of Its Unusual Glass-Forming Properties. *Science* 2008, **319**, 582-587.

32 Shephard, J. J.; Salzmann, C. G. Molecular Reorientation Dynamics Gvern the Glass Transitions of the Amorphous Ices. *J. Phys. Chem. Lett.* 2016, **7**, 2281-2285.

33 Hill, C. R.; Mitterdorfer, C.; Youngs, T. G. A.; Bowron, D. T.; Fraser, H. J.; Loerting, T. *Phys. Rev. Lett.* 2016, **116**, 215501.

34 Shi, R.; Russo, J.; Tanaka, H. Origin of the Emergent Fragile-to-Strong Transition in Supercooled Water. *Proc. Natl. Acad. Soc. USA* 2018, **115,** 9444-9449.

35 Saito, S.; Bagchi, B. Thermodynamic Picture of Vitrification of Water through Complex Specific Heat and Entropy: A Journey through "No Man's Land." *J. Chem. Phys.* 2019, **150**, 054502.

36 Kondo, T.; Kato, H. S.; Bonn, M.; Kawai, M. Deposition and Crystallization Studies of Thin Amorphous Solid Water Films on Ru(0001) and on CO-Precovered Ru(0001). *J. Chem. Phys.* 2007, **127**, 094703.

37 Souda, R.; Aizawa, T. Crystallization Kinetics of Thin Water Films on Pt(111): Effects of Oxygen and Carbon-Monoxide Adspecies. *Phys. Chem. Chem. Phys.* 2019, **21**, 1123-1130.

38 Bolina, A. S.; Wolff, A. J.; Brown, W. A. Reflection Absorption Infrared Spectroscopy and Temperature-Programmed Desorption Studies of the Adsorption and Desorption of Amorphous and Crystalline Water on a Graphite Surface. *J. Phys. Chem. B* 2005, **109**, 16836-16845.

39 Souda, R. Substrate and Surfactant Effects on the Glass-Liquid Transition of Thin Water Films. *J. Phys. Chem. B* 2006, **110**, 17524-17530.

40 McClure, S. M.; Barlow, E. T.; Akin, M. C.; Tanaka, P. L.; Safarik, D. J.; Truskett, T. M.; Mullins, C. B. Effect of Dilute Nitric Acid on Crystallization and Fracture of Amorphous Solid Water Films. *J. Phys. Chem. C* 2007, **111**, 10438-10447.

41 Badan, C.; Heyrich, Y.; Koper, M. T. M.; Juurlink, L. B. F. Surface Structure Dependence in Desorption and Crystallization of Thin Interfacial Water Films on Platinum. *J. Phys. Chem. Lett.* 2016, **7**, 1682-1685.

42 Yamauchi, T.; Mine, K.; Nakashima, Y.; Izumi, A; Namiki, A. Crystallization of D_2O Thin Films on Ru(001) Surfaces. *Appl. Surf. Sci.* 2009, **256**, 1124-1127.

43 Mehlhorn, M.; Morgenstern, K. Faceting during the Transformation of Amorphous to Crystalline Ice. *Phys. Rev. Lett.* 2007, **99**, 246101.

44 Backus, E. H. G.; Grecea, M. L.; Kleyn, A. W.; Bonn, M. Surface Crystallization of Amorphous Solid Water. *Phys. Rev. Lett.* 2004, **92**, 236101.

45 Léger, A.; Klein, J.; de Cheveigne, S.; Guinet, C.; Defourneau, D.; Belin, M. The 3.1 μm Absorption in Molecular Clouds Is Probably Due to Amorphous H_2O Ice. *Astron. Astrophys.* 1979, **79**, 256-259.

46 Hagen, W.; Tielens, A. G. G. M.: Greenberg, J. M. The Infrared Spectra of Amorphous Solid Water and Ice 1_c between 10 and 140 K. *Chem. Phys.* **1981**, **56**, 367-379.

47 Greenberg, J. M. Cosmic Dust and Our Origins. *Surf. Sci.* 2002, *500*, 793-822.

48 Boogert, A. C. A.; Gerakines, P. A.; Whittet, C. B. Observations of the Icy Universe. *Annu. Rev. Astron. Astrophys.* 2015, **53**, 541-581.

49 Sugimoto, T.; Fukutani, K. Electric-Field-Induced Nuclear-Spin Flips Mediated by Enhanced Spin-Orbit Coupling. *Nat. Phys.* 2011, **7**, 307-310.

50 Hama, T; Watanabe, N. Surface Processes on Interstellar Amorphous Solid Water: Adsorption, Diffusion, Tunneling Reactions, and Nuclear-Spin Conversion. *Chem. Rev.* 2013, **113**, 8783-8839.

51 Öberg, K. I. Photochemistry and Astrochemistry: Photochemical Pathways to Interstellar Complex Organic molecules. *Chem. Rev.* 2016, **116**, 9631-9663.

52 Smith, R. S.; Zubkov, Tykhon; Kay, B. D. The Effect of the Incident Collision Energy on the Phase and Crystallization Kinetics of Vapor Deposited Water Films. *J. Chem. Phys.* 2006, **124**, 114710.

53 Yuan, C.; Smith, R. S.; Kay, B. D. Surface and Bulk Crystallization of Amorphous Solid Water Films: Confirmation of "Top-Down" Crystallization. *Surf. Sci.* 2016, **652**, 350-354.

54 Safarik, D. J.; Meyer, R. J.; Mullins, C. B. Thickness Dependent Crystallization Kinetics of Sub-Micron Amorphous Solid Water Films. *J. Chem. Phys.* 2003, **118**, 4660-4671.

55 Speedy, R. J.; Debenedetti, P. G.; Smith, R. S.; Huang, C.; Kay, B. D. The Evaporation Rate, Free Energy, and Entropy of Amorphous Water at 150 K. *J. Chem. Phys.* 1996, **105**, 240-244.

56 Lee, D. H.; Kang, H. Acid-Promoted Crystallization of Amorphous Solid Water. *J. Phys. Chem. C* 2018, **122**, 24164-24170.

57 Kimmel, G. A.; Petrik, N. G.; Dohnálek, Z.; Kay, B. D. Crystalline Ice Growth on Pt(111): Observation of a Hydrophobic Water Monolayer. *Phys. Rev. Lett.* 2005, **95**, 166102.

58 Thürmer, K.; Bartelt, N. C. Growth of Multilayer Ice Films and the Formation of Cubic Ice Imaged with STM. *Phys. Rev. B* 2008, **77**, 195425.

59 Kimmel, G. A.; Petrik, N. G.; Dohnálek, Z.; Kay, B. D. Layer-by-Layer Growth of Thin Amorphous Solid Water Films on Pt(111) and Pd(111). *J. Chem. Phys.* 2006, **125**, 044713.

60 Zimbitas, G.; Gallagher, M. E.; Darling, G. R.; Hodgson, A. Wetting of Mixed OH H_2O Layers on Pt(111). *J. Chem. Phys.* 2008, **128**, 074701.

61 Dohnálek, Z.; Kimmel, G. A.; Ciolli, R. L.; Stevenson, K. P.; Smith, R. S.; Kay, B. D. The Effect of the Underlying Substrate on the Crystallization Kinetics of Dense Amorphous Solid Water Films. *J. Chem. Phys.* 2000, **112**, 5932-5941.

62 Zimbitas, G.; Hodgson, A. The Morphology of Thin Water Films on Pt(111) Probed by Chloroform Adsorption. *Chem. Phys. Lett.* 2006, **417**, 1-5.

63 May, R. A.; Smith, R. S.; Kay, B. D. The Molecular Volcano Revisited: Determination of Crack Propagation and Distribution During the Crystallization of Nanoscale Amorphous Solid Water Films. *J. Phys. Chem. Lett.* 2012, **3**, 327-331.

64 Yuan, C.; Smith, R. S.; Kay, B. D. Communication: Distinguishing between Bulk and Interface-Enhanced Crystallization in Nanoscale Films of Amorphous Solid Water. *J. Chem. Phys.* 2017, **146**, 031102.

65 Safarik, D. J.; Mullins, C. B. The Nucleation Rate of Crystalline Ice in Amorphous Solid Water. *J. Chem. Phys.* 2004, **121**, 6003-6010.

66 Mitchell, E. H.; Raut, U.; Teolis, B. D.; Baragiola, R. A. Prosity Effects on Crystallization Kinetics of Amorphous Solid Water: Implications for Cold Icy Objects in the Outer Solar System. *Icarus* 2017, **285**, 291-299.

67 Cox, S. J.; Kathmann, S. M.; Slater, B.; Michaelides, A. Molecular Simulations of Heterogeneous Ice Nucleation. I. Controlling Ice Nucleation through Surface Hydrophilicity. *J. Chem. Phys.* 2015, **142**, 184704.

68 Sugimoto, T.; Aiga, N.; Otsuki, Y.; Watanabe, K.; Matsumoto, Y. Emergent High-T_c Ferroelectric Ordering of Strongly Correlated and Frustrated Protons in a Heteroepitaxial Ice Film. *Nat. Phys.* 2016, **12**, 1063-1069.

69 Maté, B.; Rodríguez-Lazcano, Y.; Herrero, V. J. Morphology and Crystallization Kinetics of Compact (HGW) and Porous (ASW) Amorphous Water Ice. *Phys. Chem. Chem. Phys.* 2012, **12**, 10595-10602.

70 Buch, V.; Bauerecker, S.; Devlin, J. P.; Buck, U.; Kazimirski, J. K. Solid Water Clusters in the Size Range of Tens-Thousands of H_2O: a Combined Computational/Spectroscopic Outlook. *Int. Rev. Phys. Chem.* 2004, **23**, 375-433.

71 Otsuki, Y.; Sugimoto, T.; Ishiyama, T; Morita, A.; Watanabe, K.; Matsumoto, Y. Unveiling Subsurface Hydrogen-Bond Structure of Hexagonal Water Ice. *Phys. Rev. B* 2017, **96**, 115405.

72 Hama, T.; Ishizuka, S.; Yamazaki, T.; Kimura, Y.; Kouchi, A.; Watanabe, N.; Sugimoto, T.; Pirronello, V. Fast Crystalline Ice Formation at Extremely Low Temperature through Water/Neon Matrix Sublimation. *Phys. Chem. Chem. Phys.* 2017, **19**, 17677-17684.

73 Li, F; Skinner, J. L. Infrared and Raman Line Shapes for Ice Ih. I. Dilute HOD in H_2O and D_2O. *J. Chem. Phys.* 2010, **132**, 204505.

74 Klug, D. D.; Mishima, O.; Whalley, E. High-Density Amorphous Ice. Ⅳ. Raman Spectrum of the Uncoupled O-H and O-D Oscillators. *J. Chem. Phys.* 1987, **86**, 5323-5328.

75 Klug, D. D.; Whalley, E. The Uncoupled O-H Stretch in Ice VII. The Infrared Frequency and Integrated intensity up to 189 kbar. *J. Chem. Phys.* 1984, **81**, 1220-1228.

76 Kamb, B.; Hamilton, W.; Laplaca, S.; Prakash, A. Ordered Proton Configuration in Ice II, from Single-Crystal Neutron Diffraction. *J. Chem. Phys.* **1971**, **55**, 1934-1945.

77 Shephard, J. J.; Evans, J. S. O.; Salzmann, C. G. Structural Relaxation of Low-Density Amorphous Ice upon Thermal Annealing. *J. Phys. Chem. Lett.* 2013, **4**, 3672-3676.

78 Hage, W.; Hallbrucker, A.; Mayer, E.; Johari, G. P. Crystallization Kinetics of Water below 150 K. *J. Chem. Phys.* 1994, **100**, 2743-2747.

79 Hage, W.; Hallbrucker, A; Mayer, E.; Johari, G. P. Kinetics of Crystallizing D_2O Water near 150 K by Fourier Transform Infrared Spectroscopy and a Comparison with the Corresponding Calorimetric Studies on H_2O Water. *J. Chem. Phys.* 1995, **103**, 545-550.

80 Tainter, C. J.; Shi, L.; Skinner, J. L. Structure and OH-Stretch Spectroscopy of Low- and High-Density Amorphous Ices. *J. Chem. Phys.* 2014, **140**, 134503.

81 Ishiyama, T.; Takahashi, H.; Morita, A. Origin of Vibrational Spectroscopic Response at Ice Surface. *J. Phys. Chem. Lett.* 2012, **3**, 3001-3006.

82 Zilles, B. A.; Person, W. B. Interpretation of Infrared Intensity Changes on Molecular Complex Formation. 1. Water Dimer. *J. Chem. Phys.* 1983, **79**, 65-77.

83 Reed, A. E.; Curtiss, L. A.; Weinhold, F. Intermolecular Interactions from a Natural Bond Orbital, Donor-Accepter Viewpoint. *Chem. Rev.* 1988, **88**, 899-926.

84 Thompson, W. H.; Hynes, J. T. Frequency Shifts in the Hydrogen-Bonded OH Stretch in Halide – Water Clusters. The Importance of Charge Transfer. *J. Am. Chem. Soc.* 2000, **122,** 6278-6286.

85 Liu, H.; Wang, Y.; Bowman, J. M. Local-Monomer Calculations of the Intramolecular IR Spectra of the Cage and Prism Isomers of $HOD(D_2O)_5$ and HOD and D_2O Ice 1h. *J. Phys. Chem. B* 2014, **118**, 14124-14131.

86 Haq, S.; Harnett, J.; Hodgson, A. Growth of Thin Crystalline Ice Films on Pt(111). *Surf. Sci.* 2002, **505**, 171-182.

87 Daschbach, J. L.; Peden, B. M.; Smith, R. S.; Kay, B. D. Adsorption, Desorption, and Clustering of H_2O on Pt(111). *J. Chem. Phys.* 2004, **120**, 1516-1523.

88 Aiga, N.; Sugimoto, T.; Otsuki, Y.; Watanabe, K.; Matsumoto, Y. Origins of Emergent High-T_c Ferroelectric Ordering in Heteroepitaxial Ice Films: Sum-Frequency Generation Vibrational Spectroscopy of H_2O and D_2O Ice Films on Pt(111). *Phys. Rev. B* 2018, **97**, 075410.

89 Su, X.; Lianos, L.; Shen, Y. R.; Somorjai, G. A. Surface-Induced Ferroelectric Ice on Pt(111). *Phys. Rev. Lett.* 1998, **80**, 1533-1536.

90 Lilach, Y.; Iedema, M. J.; Cowin, J. P. Dissociation of Water Buried under Ice on Pt(111). *Phys. Rev. Lett.* 2007, **98**, 016105.

91 Fraser, H. J.; Collings, M. P.; McCoustra, M. R. S.; Williams, D. A. Thermal Desorption of Water Ice in the Interstellar Medium. *Mon. Not. R. Astron. Soc.* 2001, **327**, 1165-1172.

92 Sack, N. J.; Baragiola, R. A. Sublimation of Vapor-Deposited Water Ice below 170 K, and Its Dependence on Growth Conditions. *Phys. Rev. B* 1993, **48**, 9973-9978.

93 Kouchi, A. Vapour Pressure of Amorphous H_2O Ice and Its Astrophysical Implications. *Nature* **1**987, **330,** 550-552.

94 Smith, R. S.; Huang, C.; Wong, E. K. L.; Kay, B. D. The Molecular Volcano: Abrupt CCl_4 Desorption Driven by the Crystallization of Amorphous Solid Water. *Phys. Rev. Lett.* 1997, **79**, 909.

95 McClure, S. M.; Barlow, E. T.; Akin, M. C.; Safarik, D. J.; Truskett, T. M.; Mullins C. B. Transport in Amorphous Solid Water Films: Implications for Self-Diffusivity. *J. Phys. Chem. B* 2006, **110**, 17987-17997.

96 Sumith, YD.; Maroo, S. C. Surface-Heating Algorithm for water at Nanoscale. *J. Phys. Chem. Lett.* **2**015, **6**, 3765-3769.

97 Nagao, M.; Watanabe, K.; Matsumoto, Y. Ultrafast Vibrational Energy Transfer in the Layers of D_2O and CO on Pt(111) Studied with Time-Resolved Sum-Frequency-Generation Spectroscopy. *J. Phys. Chem. C* 2009, **113**, 11712-11719.

98 Fitzner, M.; Sosso, G. C.; Cox, S. J.; Michaellides, A. The Many Faces of Heterogeneous Ice Nucleation: Interplay Between Surface Morphology and Hydrophobicity. *J. Am. Chem. Soc.* 2015, **137**, 13658-13669.

99 Zhang, X. X.; Chen, M.; Fu, M. Impact of Surface Nanostructure on Ice Nucleation. *J. Chem. Phys.* 2014, **141,** 124709.

100 Feibelman, P. J.; Kimmel, G. A.; Smith, R. S.; Petrik, N. G.; Zubkov, T.; Kay, B. D. A Unique Vibrational Signature of Rotated Water Monolayers on Pt(111): Predicted and Observed. *J. Chem. Phys.* 2011, **134**, 204702.

101 Kimmel, G. A.; Zubkov, T.; Smith, R. S.; Petrik, N. G.; Kay, B. D. Turning Things Downside Up: Adsorbate Induced Water Flipping on Pt(111). *J. Chem. Phys.* 2014, **141**, 18C515.

102 Nie, S.; Feibelman, P. J.; Bartelt, N. C.; Thürmer, K. Pentagons and Heptagons in the First Water Layer on Pt(111). *Phys. Rev. Lett.* 2010, **105**, 026102.

103 Feibelman, P. J.; Bartelt, N. C.; Nie, S.; Thürmer, K. Interpretation of High-Resolution Images of the Best-Bound Wetting Layers on Pt(111). *J. Chem. Phys.* 2010, **133**, 154703.

104 Wagner, F. T.; Moylan, T. E. A Comparison between Water Adsorbed on Rh(111) and Pt(111), with and without Predosed Oxygen. *Surf. Sci.* 1987, **191**, 121-146.

105 Sugimoto, T.; Otsuki, Y.; Ishiyama, T.; Morita, A.; Watanabe, K.; Matsumoto, Y. Topologically Disordered Mesophase at the Topmost Surface Layer of Crystalline Ice between 120 and 200 K. *Phys. Rev. B* 2019, **99**, 121402(R).

106 Kouchi, A.; Greenberg, J. M.; Yamamoto, T.; Mukai, T. Extremely Low Thermal Conductivity of Amorphous Ice: Relevance to Comet Evolution. *Astrophys. J.* 1992, **388**, L73-L76.

107 Avrami, M. Kinetics of Phase Change. I General Theory. *J. Chem. Phys.* 1939, **7***,* 1103-1112.

108 Avrami, M. Kinetics of Phase Change. II Transformation-Time Relations for Random Distribution of Nuclei. *J. Chem. Phys.* 1940, **8***,* 212-224.

109 Avrami, M. Kinetics of Phase Change. III Granulation, Phase Change, and Microstructure. *J. Chem. Phys.* 1941, **9**, 177-184.

110 Moghadam, M. M.; Pang, E. L.; Philippe, T.; Voorhees, P. W. Simulation of Phase Transformation Kinetics in Thin Films under a Constant Nucleation Rate. *Thin Solid Films* 2016, **612**, 437-444.

111 Pang, E. L.; Vo, N. Q.; Philippe, T.; Voorhees, P. W. Modeling Interface-Controlled Phase Transformation Kinetics in Thin Films. *J. Appl. Phys.* 2015, **117**, 175304.

112 Očenášek, J.; Novák, P.; Agbo, S. Finite-Thickness Effect on Crystallization Kinetics in Thin Films and its Adaption in the Johnson-Mehl-Avrami-Kolmogorov Model. *J. Appl. Phys.* 2014, **115**, 043505.

113 Schultz, J. M. Effect of Specimen Thickness on Crystallization Rate. *Macromolecules* 1996, **29**, 3022-3024.

114 Moore, E. B.; Molinero, V. Structural Transformation in Supercooled Water Controls the Crystallization Rate of Ice. *Nature* 2011, **489**, 506-509.

115 Zasetsky, A. Y.; Petelina, S. V.; Svishechev, I. M. Thermodynamics of Homogeneous Nucleation of Ice Particles in the Polar Summer Mesosphere. *Atmos. Chem. Phys.* 2009, **9**, 965-971.

116 Reinhardt, A.; Doye, J. P. K. Free Energy Landscapes for Homogeneous Nucleation of Ice for a Monatomic Water Model. *J. Chem. Phys.* 2012, **136**, 054501.

117 Sanz, E.; Vega, C.; Espinosa, J. R.; Caballero-Bernal, R.; Abascal, J. L. F.; Valeriani, C. Homogeneous Ice Nucleation at Moderate Supercooling from Molecular Simulation. *J. Am. Chem. Soc.* 2013, **135**, 15008-15017.

118 Matsumoto, M.; Saito, S.; Ohmine, I. Molecular Dynamics Simulation of the Ice Nucleation and Growth Process Leading to Water Freezing. *Nature* 2002, **416**,409-413.

119 Shirai, K.; Fazio, G.; Sugimoto, T.; Selli, D.; Ferraro, L.; Watanabe, K.; Haruta, M.; Ohtani, B.; Kurata, H.; Di Valentin, C.; Matsumoto, Y. Water-Assisted Hole Trapping at the Highly Curved Surface of Nano-TiO_2 Photocatalyst. *J. Am. Chem. Soc.* 2018, **140**, 1415-1422.

120 Tsuruoka, K.; Koyasu, K.; Hirabayashi, S.; Ichihashi, M.; Tsukuda, T. Size-Dependent Polymorphism in Aluminum Carbide Cluster Anions $Al_nC_2^-$: Formation of Acetylide-Containing Structures. *J. Phys. Chem. C* 2018, **122**, 8341-8347.

TOC one sentence of text

Film-size-dependent homogeneous crystallization phenomenon of nanoscopic amorphous films is demonstrated with a clear relationship between crystallization kinetics and microscopic structural changes.

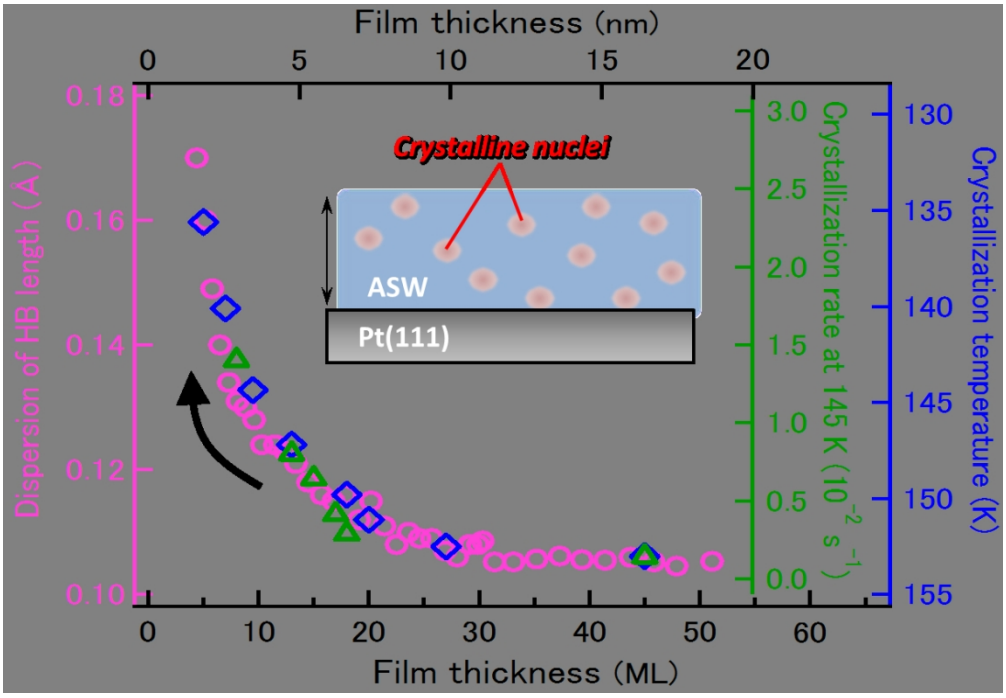
Film thickness (nm)
0
5
10
15
20
Crystalline nuclei
ASW
Pt(111)
Dispersion of HB length (Å)
0.18
0.16
0.14
0.12
0.10
Crystallization rate at 145 K (10^{-2} s^{-1})
3.0
2.5
2.0
1.5
1.0
0.5
0.0
Crystallization temperature (K)
130
135
140
145
150
155
0
10
20
30
40
50
60
Film thickness (ML)